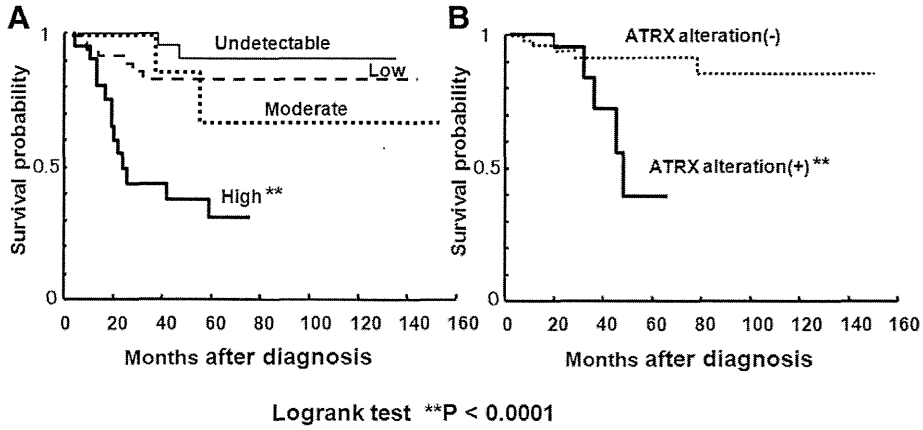

Fig. 2. Kaplan–Meier cumulative survival curves for patients with telomerase activity levels and ATRX alterations. A: Survival curves for patients with high, moderate, and low levels of telomerase activity in tumor samples. These data were analyzed in our previous report [9]. Patients with NBLs having high telomerase activity (n = 22, thick solid line) showed significantly poorer prognoses than those with moderate (n = 54) or low (n = 45) activity ($P < 0.001$). However, patients without high telomerase activity did not usually show good outcomes. B: Survival curve of patients with NBL tumors with *ATRX* mutation or deletion (n = 10) and that of the remaining patients without high telomerase activity (n = 88). The case with the *DAXX* mutation and the one *ATRX* deleted case were excluded in this analysis because these tumors had high telomerase activity. In NBLs without high telomerase activity, patients with altered *ATRX* tumors had significantly worse survival rates ($P < 0.001$). Length of follow-up in all cases was 69 ± 17 months (n = 121).

subgroups has now been attempted. *ATRX* or *DAXX* mutated NBLs might become a new subgroup for targeted molecular therapy.

Acknowledgments

This research was partially supported by Grant-in-Aids for Scientific Research (A) (No. 13313631 and 13370806) from the Ministry of Education, Culture, Sports, Science, and Technology and for Cancer Research by that (13801449) from theMinistry of Health, Labor, and Welfare of the Government of Japan.

We thank the Japanese pediatric oncologists and surgeons for providing tissue specimens and the clinical data of neuroblastoma patients under written informed consent.

References

[1] Hiyama E, Iehara T, Sugimoto T, et al. Effectiveness of screening for neuroblastoma at 6 months of age: a retrospective population-based cohort study. Lancet 2008;371:1173–80.
[2] Hiyama E, Hiyama K. Diagnostic and prognositic molecular markers in neuroblastoma. Kerala: Transworld Research Network; 2009 135–62.
[3] Pugh TJ, Morozova O, Attiyeh EF, et al. The genetic landscape of high-risk neuroblastoma. Nat Genet 2013;45:279–84.
[4] Deyell RJ, Attiyeh EF. Advances in the understanding of constitutional and somatic genomic alterations in neuroblastoma. Cancer Genet 2011;204:113–21.
[5] Mosse YP, Laudenslager M, Longo L, et al. Identification of ALK as a major familial neuroblastoma predisposition gene. Nature 2008;455:930–5.
[6] Trochet D, Bourdeaut F, Janoueix-Lerosey I, et al. Germline mutations of the paired-like homeobox 2B (PHOX2B) gene in neuroblastoma. Am J Hum Genet 2004;74:761–4.
[7] Hiyama E, Hiyama K, Yokoyama T, et al. Correlating telomerase activity levels with human neuroblastoma outcomes. Nat Med 1995;1:249–55.
[8] Hiyama E, Hiyama K, Shay JW, et al. Immunhistochemical detection of telomerase (hTERT) protein in human cancer tissues and a subset of cells in normal tissues. Neoplasia 2001;3:17–26.
[9] Onitake Y, Hiyama E, Kamei N, et al. Telomere biology in neuroblastoma: telomere binding proteins and alternative strengthening of telomeres. J Pediatr Surg 2009;44:2258–66.
[10] Cheung NK, Zhang J, Lu C, et al. Association of age at diagnosis and genetic mutations in patients with neuroblastoma. JAMA 2012;307:1062–71.
[11] Brodeur GM, Pritchard J, Berthold F, et al. Revisions of the international criteria for neuroblastoma diagnosis, staging, and response to treatment [see comments]. J Clin Oncol 1993;11:1466–77.
[12] Shimada H, Ambros IM, Dehner LP, et al. The International Neuroblastoma Pathology Classification (the Shimada system). Cancer 1999;86:364–72.
[13] Sawaguchi S, Kaneko M, Uchino J, et al. Treatment of advanced neuroblastoma with emphasis on intensive induction chemotherapy: a report from the Study Group of Japan. Cancer 1990;66:1879–87.
[14] Yuan E, Haghighi F, White S, et al. A single nucleotide polymorphism chip-based method for combined genetic and epigenetic profiling: validation in decitabine therapy and tumor/normal comparisons. Cancer Res 2006;66:3443–51.
[15] Zhang J, Benavente CA, McEvoy J, et al. A novel retinoblastoma therapy from genomic and epigenetic analyses. Nature 2012;481:329–34.
[16] Heaphy CM, de Wilde RF, Jiao Y, et al. Altered telomeres in tumors with ATRX and DAXX mutations. Science 2011;333:425.
[17] Hiyama E, Yokoyama T, Hiyama K, et al. Alteration of telomeric repeat length in adult and childhood solid neoplasias. Int J Oncol 1995;6:13–6.
[18] Hashimoto M, Kyo S, Masutomi K, et al. Analysis of telomeric single-strand overhang length in human endometrial cancers. FEBS Lett 2005;579:2959–64.
[19] Stewart SA, Ben-Porath I, Carey VJ, et al. Erosion of the telomeric single-strand overhang at replicative senescence. Nat Genet 2003;33:492–6.
[20] Kim NW, Piatyszek MA, Prowse KR, et al. Specific association of human telomerase activity with immortal cells and cancer. Science 1994;266:2011–5.
[21] Piatyszek MA, Kim NW, Weinrich SL, et al. Detection of telomerase activity in human cells and tumors by a telomeric repeat amplification protocol (TRAP). Methods Cell Sci 1995;17:1–15.
[22] Hiyama E, Yamaoka H, Kondo S, et al. Heterogeneous subgroups in human neuroblastoma for clinically relevant risk stratification. Pediatr Surg Int 2007;23:1051–8.
[23] Hiyama E, Hiyama K, Ohtsu K, et al. Telomerase activity in neuroblastoma: is it a prognostic indicator of clinical behavior? Eur J Cancer 1997;33:1932–6.
[24] Reynolds CP, Zuo JJ, Hong CM, et al. Telomerase RNA expression in neuroblastoma correlates with high stage and clinical outcome. Proc A Assoc Cancer Res 1996;37:199.
[25] Hiyama E, Hiyama K, Yokoyama T, et al. Length of telomeric repeats in neuroblastoma: correlation with prognosis and other biological characteristics. Jpn J Cancer Res 1992;83:159–64.
[26] Lovejoy CA, Li W, Reisenweber S, et al. Loss of ATRX, genome instability, and an altered DNA damage response are hallmarks of the alternative lengthening of telomeres pathway. PLoS Genet 2012;8:e1002772.
[27] Bower K, Napier CE, Cole SL, et al. Loss of wild-type ATRX expression in somatic cell hybrids segregates with activation of Alternative Lengthening of Telomeres. PLoS One 2012;7:e50062.
[28] Sridhar S, Al-Moallem B, Kamal H, et al. New insights into the genetics of neuroblastoma. Mol Diagn Ther 2013;17:63–9.
[29] Brodeur GM, Seeger RC, Schwab M, et al. Amplification of N-myc in untreated human neuroblastoma correlated with advanced stage. Science 1984;224:1121–4.
[30] Wylie L, Philpott A. Neuroblastoma progress on many fronts: the Neuroblastoma Research Symposium. Pediatr Blood Cancer 2012;58:649–51.
[31] Ogura T, Hiyama E, Kamei N, et al. Clinical feature of anaplastic lymphoma kinase-mutated neuroblastoma. J Pediatr Surg 2012;47:1789–96.
[32] Hiyama E, Hiyama K. Molecular and biological heterogeneity in neuroblastoma. Curr Genomics 2005;6:319–32.

Genes to Cells

FAST-id system for enrichment of cells with TALEN-induced mutations and large deletions

Daisuke Tokumasu[1†], Tetsushi Sakuma[1†], Yoko Hayashi[2], Sayaka Hosoi[1], Eiso Hiyama[2] and Takashi Yamamoto[1*]

[1]*Department of Mathematical and Life Sciences, Graduate School of Science, Hiroshima University, 1-3-1 Kagamiyama, Higashi-Hiroshima, Hiroshima 739-8526, Japan*
[2]*Natural Science Center for Basic Research and Development (N-BARD), Hiroshima University, 1-2-3 Kasumi, Minami-ku, Hiroshima 734-8551, Japan*

Transcription activator-like effector nuclease (TALEN)-mediated genome editing is a powerful technique for analyzing gene functions in various cells and organisms. At target loci, TALENs can not only introduce short insertions and deletions, but also yield large deletions through the use of two TALEN pairs. Here, we report easy and efficient methods for enrichment of cells with TALEN-induced mutations and large deletions. First, we established the fluorescence-activated sorting of TALEN-induced deletions (FAST-id) system that enabled fluorescence-activated cell sorting-mediated enrichment of cells with TALEN-induced mutations. In the FAST-id system, either EGFP or mCherry and TALENs were co-expressed. Using dual fluorescence selection, both left and right TALEN-expressing cells were easily concentrated, resulting in enrichment of TALEN-mediated mutated cells. Next, to apply the FAST-id system to enrichment of cells with large deletions, we developed the fast unification of separate endonucleases (FUSE) method for assembly of two TALENs into a single expression vector. Using the FUSE method, we easily obtained a TALEN pair-expressing plasmid driven by a single promoter. By combining the FAST-id system and FUSE method, cells with large deletions were efficiently enriched. To the best of our knowledge, this is the first report of enrichment of cells with TALEN-induced large deletions.

Introduction

Recently, targeted genome engineering using engineered nucleases, including zinc finger nucleases (ZFNs) and transcription activator-like effector nucleases (TALENs), has attracted attention as an effective tool in various cultured cells or organisms (Urnov *et al.* 2010; Joung & Sander 2013). Engineered nucleases are composed of a sequence-specific DNA-binding domain and a nonspecific DNA cleavage domain derived from the FokI restriction endonuclease, which can induce double-strand breaks (DSBs) into target sequences. Engineered nuclease-induced DSBs can be repaired by nonhomologous end-joining (NHEJ) or homology-directed repair (HDR). Error-prone NHEJ repair frequently leads to the introduction of short insertions and deletions (indels), frequently resulting in gene disruption via a frameshift (Santiago *et al.* 2008). In the template-dependent repair pathway, HDR, insertion of exogenous genes into the genome is achieved using a donor template containing ~1-kb homology arms adjacent to the target sequence (Moehle *et al.* 2007; Hockemeyer *et al.* 2011). Furthermore, DSBs can be introduced into two sites through the use of two pairs of ZFNs or TALENs, resulting in chromosomal deletions, inversions, and duplications when two DSB sites are on the same chromosome (Lee *et al.*

Communicated by: Masayuki Miura
**Correspondence:* tybig@hiroshima-u.ac.jp
†These authors contributed equally to this study.

DOI: 10.1111/gtc.12142

2010, 2012) and chromosomal translocations when the sites are on different chromosomes (Brunet *et al.* 2009; Piganeau *et al.* 2013).

To facilitate the use of TALEN technology, it is absolutely necessary to develop easy and efficient methods for selecting TALEN-induced mutated cells. Currently, several methods have been reported for enrichment of ZFN- or TALEN-induced mutated cells. A surrogate reporter system (Kim *et al.* 2011, 2013a) can be used to validate the activity of ZFNs or TALENs in living cells and to select potentially mutated cells by sorting based on fluorescence intensity, magnetic separation, or antibiotic selection. As another method, enrichment of TALEN-induced mutated cells by co-expressing TALENs and fluorescent proteins and subsequent sorting of TALEN-expressing cells based on fluorescence intensity was reported (Ding *et al.* 2013). However, there are no reports regarding methods for enrichment of chromosomally rearranged cells using two TALEN pairs.

Here, we report efficient methods for enrichment of cells with TALEN-induced mutations and chromosomal deletions. We constructed vectors to visualize the expression levels of TALENs on the basis of fluorescence intensity. Subsequently, we showed that sorting of cells exhibiting high expression of TALENs based on fluorescence intensity using fluorescence-activated cell sorting (FACS) enabled enrichment of cells with TALEN-induced mutations or large deletions.

Results

Enrichment of cells with TALEN-induced mutations by FACS

To select cells in which mutations such as indels are introduced into the target sites by TALENs, it is necessary to distinguish cells showing high expression of both left and right TALENs from a variety of cells expressing either the left or right TALEN alone or neither TALEN. To monitor the expression of a TALEN pair, we planned to construct two types of plasmid vectors in which a gene for a fluorescent protein (mCherry or EGFP) was bicistronically linked to a gene for one TALEN (L or R) via the 'self-cleaving' 2A peptide sequence (Fig. 1A). Following transfection of these plasmids into mammalian cells, it was expected that both the TALEN and the fluorescent protein would be expressed as separate proteins. Therefore, by sorting of positive cells for both mCherry and EGFP fluorescence, we can easily select

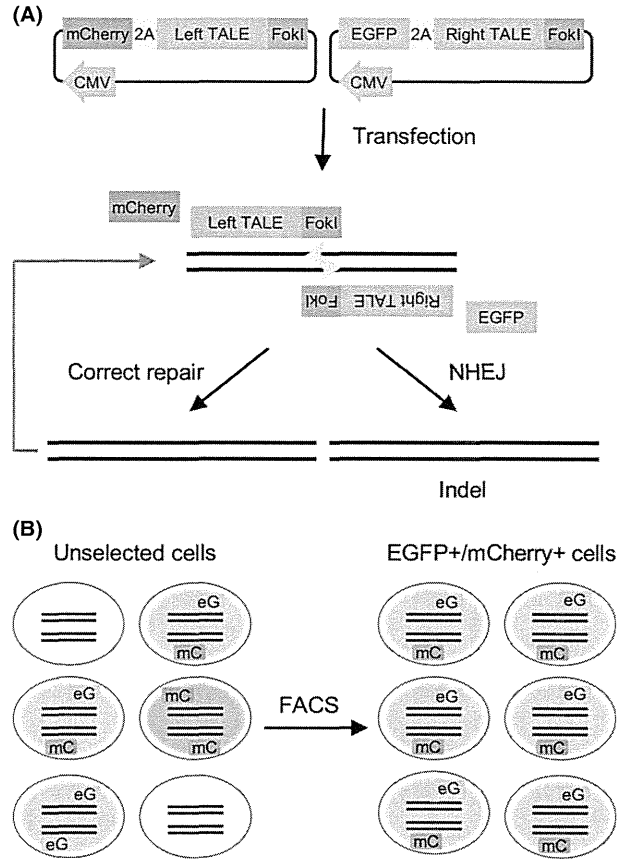

Figure 1 Schematic overview of the fluorescence-activated sorting of TALEN-induced deletions (FAST-id system). (A) Scheme of TALEN-mediated mutagenesis using the FAST-id system. A TALEN and either EGFP or mCherry are co-expressed and translated as individual proteins, which allows visualization of the expression level of the TALEN by the fluorescence intensity. The NHEJ pathway often introduces insertions and/or deletions (indels, red lines) at the TALEN target site. CMV, cytomegalovirus promoter; 2A, 2A sequence. (B) Scheme of enrichment of cells with TALEN-induced mutations. Fluorescence intensity-dependent cell sorting using fluorescence-activated cell sorting enables selection of cells showing high expression of both the left and right TALENs, resulting in enrichment of cells with TALEN-induced mutations. eG, EGFP; mC, mCherry.

cells expressing both the left and right TALENs, which are expected to introduce indel mutations at the target site (Fig. 1B). We referred to this system as the 'fluorescence-activated sorting of TALEN-induced deletions (FAST-id)' system.

To investigate whether cells with TALEN-induced mutations can be efficiently enriched by the FAST-id system, we constructed fluorescent protein-2A-TALEN plasmids targeting the human hypoxanthine

phosphoribosyltransferase 1 (*HPRT1*) locus (*HPRT1*_B TALEN), transfected these plasmids into HCT116 cells, and performed flow cytometric analyses. *HPRT1* is an X-linked gene, and HCT116 cells have only one copy of this gene in their genome. As shown in Fig. 2A, the transfected cells showed various intensities of EGFP and mCherry fluorescence, indicating that there were variations in the TALEN expression levels in the transfected cells (Fig. 2A, left panel). To evaluate the extent of the TALEN-induced mutations, we carried out PCR amplification of the target region of the *HPRT1*_B TALEN using genomic DNA extracted from unselected cells and EGFP−/mCherry− and EGFP+/mCherry+ cells (Fig. 2A, squares), and examined each mutation rate by restriction fragment length polymorphism (RFLP) analysis after digestion with the restriction enzyme Hpy188I, which has a site located in the middle of the *HPRT1*_B TALEN spacer region. If a mutation was introduced into the

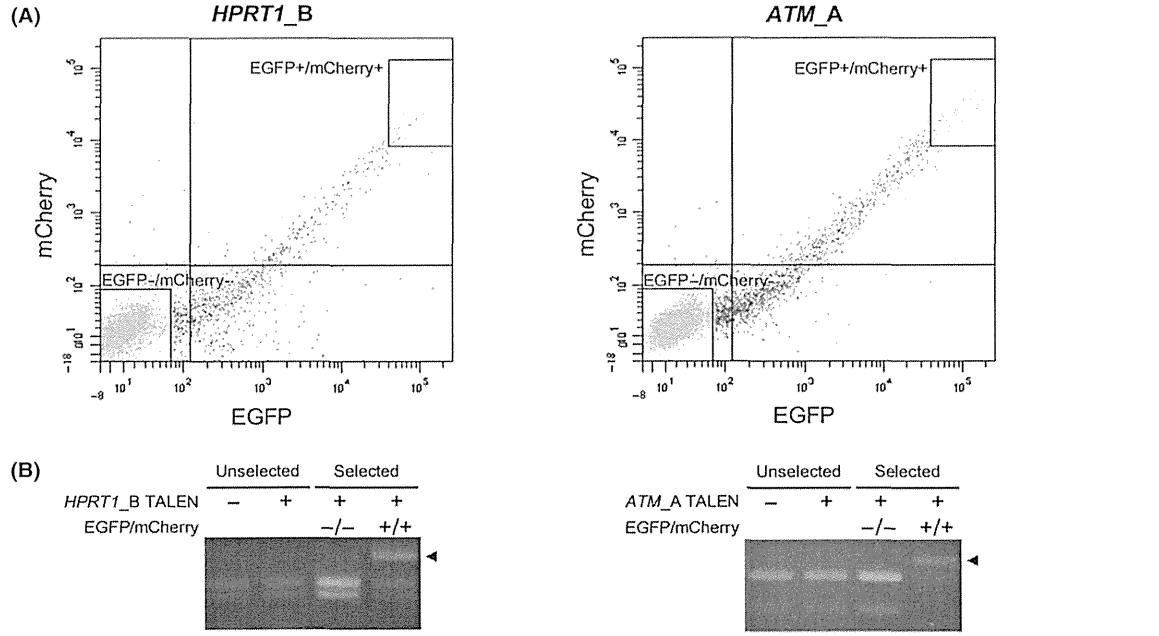

(C)

*HPRT1*_B Unselected cells 20%(3/15)

```
agtgatagatCCATTCCTATGACTGTAGATtttatcagactgaagAGCTATTGTGTGAGTATatttaatata WT
agtgatagatCCATTCCTATGACTGTAGATttctat----cacagAGCTATTGTGTGAGTATatttaatata
agtgatagatCCATTCCTATGACTGTAGATtttatcagactggagAGCTATTGTGTGAGTATatttaatata
agtgatagatCCATTCCTATGACTGTAGATtttatcagactgaagAGCTgTTGTGTGAGTATatttaatata
```

*HPRT1*_B EGFP+/mCherry+ cells 83%(10/12)

```
agtgatagatCCATTCCTATGACTGTAGATtttatcagactgaagAGCTATTGTGTGAGTATatttaatata WT
agtgatagatCCATTCCTATGACTGTAGATttttat---actgaagAGCTATTGTGTGAGTATatttaatata x2
agtgatagatCCATTCCTATGACTGTAGATttta-------gaagAGCTATTGTGTGAGTATatttaatata x2
agtga-------------------------------------------------------------ta x2
agtgatagatCCATTCCTATGACTGTAGATttttatc------aagAGCTATTGTGTGAGTATatttaatata
agtgatagatCCATTCCTATGACTGTAGATttttatc-------agAGCTATTGTGTGAGTATatttaatata
agtgatagatCCATTCCTATGACT----------------tgaagAGCTATTGTGTGAGTATatttaatata
agtgatagatCCATTCCTATGAC-----------------tgaagAGCTATTGTGTGAGTATatttaatata
```

*ATM*_A Unselected cells 20%(3/15)

```
aaccatgagtCTAGTACTTAATGATCtgcttatctgctgccGTCAACTAGAACATGATagagctacag WT
aaccatgagtCTAGTACTTAATGAT----------ctgccGTCAACTAGAACATGATagagctacag
aaccatgagtCTAGTACTTgATGATCtgcttatctgctgccGTCAACTAGAACATGATagagctacag
aaccatgagtCTAGTACTTAAcGATCtgcttatctgctgccGTCAACTAGAACATGATagagctacag
```

*ATM*_A EGFP+/mCherry+ cells 100%(14/14)

```
aaccatgagtCTAGTACTTAATGATCtgcttatctgctgccGTCAACTAGAACATGATagagctacag WT
aaccatgagtCTAGTACTTAATGATCtgctta------gccGTCAACTAGAACATGATagagctacag x4
aac---------------------------------------CTAGAACATGATagagctacag x4
aaccatgagtCTAGTACTTAATGATC----------------AACTAGAACATGATagagctacag x4
------------------------------------------AACTAGAACATGATagagctacag -185
aaccatgagtCTAGTACTTAATGATCtgctta-----tgccGTCAACTAGAACATGATagagctacag
```

Figure 2 Enrichment of cells with TALEN-induced mutations. (A) Flow cytometric analyses of HCT116 cells transfected with *HPRT1*_B (left panel) or *ATM*_A (right panel) TALEN-encoding plasmids. Cells showing high expression (EGFP+/mCherry+) and minimal expression (EGFP−/mCherry−) were collected (squares). Indexes of numbers and percentages of collected cells are listed in Table S5 in Supporting Information. Vertical and horizontal lines indicate background fluorescence levels of EGFP and mCherry, respectively. (B) RFLP analyses of mutations induced by *HPRT1*_B (left panel) or *ATM*_A (right panel) TALENs. The genomic PCR products of unselected, EGFP−/mCherry−, and EGFP+/mCherry+ cells transfected with the *HPRT1*_B or *ATM*_A TALEN-encoding plasmids or untransfected cells were purified, digested, and analyzed by agarose gel electrophoresis. The arrowheads indicate the expected positions of the undigested products. (C) Sequences observed in unselected and EGFP+/mCherry+ cells transfected with the *HPRT1*_B or *ATM*_A TALEN-encoding plasmids. The wild-type sequence of *ATM* or *HPRT1* is shown at the top with the TALEN target sequence (capital letters with underlines). Deletions are indicated by dashes.

spacer region of the *HPRT1*_B TALEN target site, mutated alleles would be detected as resistant fragments against Hpy188I digestion. As shown in Fig. 2B, an Hpy188I-resistant fragment was strongly detected in the PCR products from EGFP+/mCherry+ cells, but scarcely detected among the PCR products from unselected cells and EGFP−/mCherry− cells (Fig. 2B, left panel). Similarly, we constructed fluorescent protein-2A-TALEN plasmids targeting the ataxia–telangiectasia mutated (*ATM*) locus (*ATM*_A TALEN). *ATM* is an autosomal gene, and HCT116 cells have two copies of this gene in the genome. After transfection of these plasmids and fluorescence-mediated cell sorting (Fig. 2A, right panel), we carried out RFLP analysis with the restriction enzyme Fnu4HI. Consistent with the results for the *HPRT1* gene, a restriction enzyme-resistant fragment was observed in the PCR products from EGFP+/mCherry+ cells, but hardly observed among the PCR products from unselected and EGFP−/mCherry− cells (Fig. 2B, right panel).

Next, to investigate the rate and context of the mutations, we analyzed the mutations introduced into the target sites by the TALENs. DNA fragments amplified by PCR using genomic DNA extracted from unselected or EGFP+/mCherry+ cells were subcloned, and their nucleotide sequences were determined (Fig. 2C). We found that the mutation frequency of the *HPRT1*_B TALEN target site in EGFP+/mCherry+ cells was 83%, whereas that in unselected cells was 20%, showing 4.2-fold enrichment of cells with TALEN-induced mutations (Table 1). Similarly, in the fluorescent protein-2A-*ATM*_A TALEN plasmid-transfected cells, the mutation frequency in EGFP+/mCherry+ cells was 100%, whereas that in unselected cells was 20%, showing 5-fold enrichment of cells with indel mutations (Table 1). These results suggest that the FAST-id system is efficient for enrichment of cells with TALEN-mediated mutations.

Establishment of a unification system for TALEN expression vectors

Although systems for enrichment of cells with TALEN-induced indel mutations have been reported (Kim *et al.* 2011, 2013a; Ding *et al.* 2013), there are no previous reports regarding systems for enrichment of cells with TALEN-mediated chromosomal deletions. For TALEN-mediated chromosomal deletions, it is necessary to express two pairs of TALENs in cells to cut two different sites on the same chromosome. To monitor the expression levels of the two pairs of TALENs and select cells using the FAST-id system, the expression of four kinds of fluorescent proteins would be required. However, it is thought that the transfection efficiency of four types of fluorescent protein-2A-TALEN plasmids may be low. In addition, it is difficult to sort cells expressing two pairs of TALENs on the basis of four kinds of fluorescence intensity, because the fluorescence spectra must overlap. Therefore, we planned to construct a vector expressing a fluorescent protein and a pair of TALENs in a single plasmid to allow monitoring of the expression of the TALEN pair by a single fluorescent protein, such that we can select cells showing high expression of two pairs of TALENs using only two fluorescent proteins.

To realize the above-described system, we established the 'fast unification of separate endonucleases (FUSE)' method. In the FUSE method, we construct left and right TALEN expression vectors as separate vectors at the first step, and subsequently unify these vectors into a single expression vector by digestion and ligation at the second step (Fig. 3A). In the left TALEN expression vector, a fluorescent protein gene is ligated to the left TALEN gene via the 2A sequence, whereas in the right TALEN expression vector, the 2A sequence is inserted in the upstream of the right TALEN gene. Furthermore, BamHI sites are inserted in the upstream of the stop codon of the

Table 1 Comparison of mutation frequencies in unselected and EGFP+/mCherry+ cells

TALEN	Mutation frequency (%)		Fold enrichment	Types of mutation
	Unselected	EGFP+/mCherry+		
*HPRT1*_B	20	83	4.2	Indel
*ATM*_A	20	100	5.0	Indel
*HPRT1*_B + *HPRT1*_E	3	41	13.7	Chromosomal deletion
*ATM*_A + *ATM*_D	11	77	7.0	Chromosomal deletion

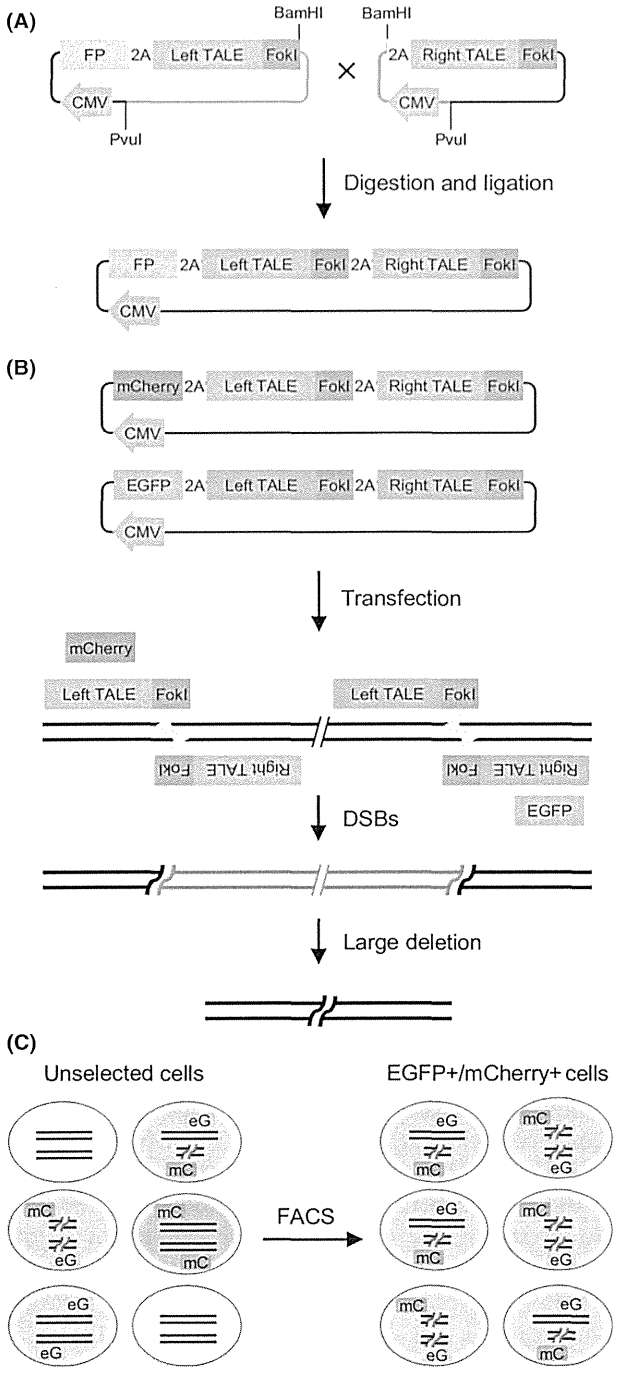

Figure 3 Schematic overview of the combined system using the fast unification of separate endonucleases (FUSE) method and fluorescence-activated sorting of TALEN-induced deletions (FAST-id) system. (A) Scheme of the FUSE method. Left and right TALEN expression vectors are constructed separately and subsequently unified by double digestion with BamHI and PvuI followed by ligation. FP, fluorescent protein. (B) Scheme for combining the FUSE method and FAST-id system. Transfection of two kinds of one TALEN pair-encoding plasmids created by the FUSE method into cells enables the introduction of two double-strand breaks on the target chromosome, resulting in the introduction of a large deletion. (C) Scheme of enrichment of chromosomally deleted cells. Fluorescence intensity-dependent cell sorting using fluorescence-activated cell sorting enables selection of cells showing high expression of the two TALEN pairs, resulting in enrichment of cells with the chromosomal deletion.

left TALEN gene and between the start codon and the 2A sequence in the right TALEN expression vector for the assembly of both TALENs. Importantly, we can evaluate the activity of these TALEN expression vectors by a single-strand annealing (SSA) assay (Sakuma *et al.* 2013), because they retain the structure of a TALEN expression vector. A pair of TALENs, whose activity is confirmed, can be unified quickly by BamHI digestion and ligation along with removal of unnecessary start and stop codons to form a single gene encoding fluorescent protein-2A-left TALEN-2A-right TALEN. Although the footprint of the BamHI site (5′-GGATCC-3′) is retained in front of the 2A-right TALEN, it functions as part of a GSG linker at the N-terminus of the 2A peptide. Thus, we can enable seamless ligation of the left and right TALEN array into a single expression vector (Fig. 3A) to efficiently obtain cells with two DSB-induced large deletions (Fig. 3B).

Enrichment of cells with TALEN-induced large deletions using the FUSE method and FAST-id system

Next, we carried out the enrichment of chromosomally deleted cells by combining the FUSE method and FAST-id system (Fig. 3C). We planned to construct two pairs of TALENs targeting different regions of the *HPRT1* locus (*HPRT1*_B and *HPRT1*_E, Fig. 4A). After confirming the mutagenic frequency using separate TALEN expression vectors by the SSA assay, we used the FUSE method to unify the *HPRT1*_B TALEN pair into a single expression vector containing the mCherry sequence and the *HPRT1*_E TALEN pair targeting approximately 1100-bp upstream of the *HPRT1*_B TALEN target site into a single expression vector containing the EGFP sequence. We then examined the mutagenic frequencies of the *HPRT1*_B and *HPRT1*_E TALENs as single expression vectors or separate

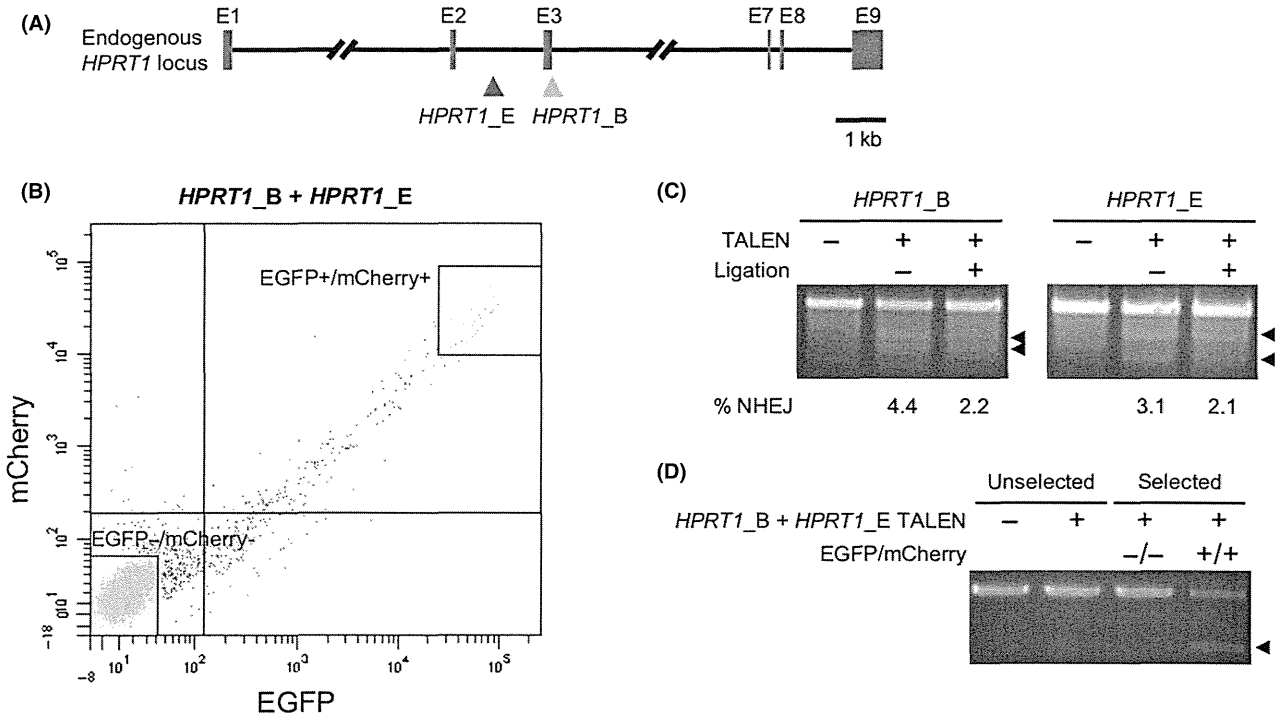

(E) *HPRT1*_B + *HPRT1*_E TALEN (Unselected cells)

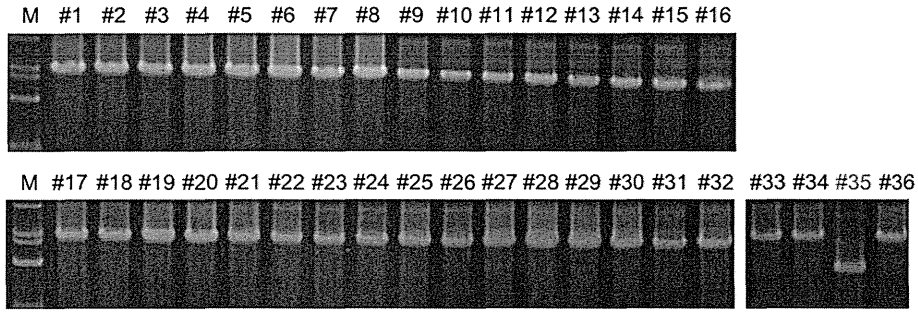

***HPRT1*_B + *HPRT1*_E Unselected cells** 3%(1/36)

```
       HPRT1_E TALEN Left site                                    HPRT1_B TALEN Right site
agcattctgtCTTATGGAGATACCATAactgatttaaccagt..1139bp..tttatcagactgaagAGCTATTGTGTGAGTATatttaatata WT
agcattctgtCTTATGGAGATACCATAactg-ttt----------------------------actgaagAGCTATTGTGTGAGTATatttaatata
```

(F) *HPRT1*_B + *HPRT1*_E TALEN (EGFP+/mCherry+ cells)

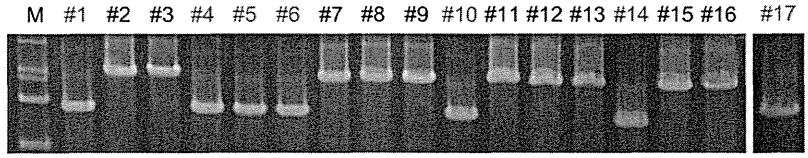

***HPRT1*_B + *HPRT1*_E EGFP+/mCherry+ cells** 41%(7/17)

```
       HPRT1_E TALEN Left site                                    HPRT1_B TALEN Right site
agcattctgtCTTATGGAGATACCATAactgatttaaccagt..1139bp..tttatcagactgaagAGCTATTGTGTGAGTATatttaatata WT
agcattctgtCTTATGGAGATACCATAactga-------------------------------aagAGCTATTGTGTGAGTATatttaatata x2
agcattctgtCTTATGGAGATACCATAactga-------------------------------agAGCTATTGTGTGAGTATatttaatata x2
agcattctgtCTTATGGAGATACCATAactga--------------------------------gAGCTATTGTGTGAGTATatttaatata
agcattctgtCTTATGGAGATACCATAactgaat------------------------------aagAGCTATTGTGTGAGTATatttaatata
agcattctgtCTTATGGAGATACCA---ctgat------------------------------aagAGCTATTGTGTGAGTATatttaatata
```

Figure 4 Enrichment of chromosomally deleted cells at the *HPRT1* locus. (A) Schematic illustration of the human *HPRT1* gene. The target sites of the *HPRT1*_B and *HPRT1*_E TALENs are shown by the yellow and red arrowheads, respectively. E, exon. (B) Flow cytometric analysis of HCT116 cells transfected with the *HPRT1*_B and *HPRT1*_E TALEN-encoding plasmids. Cells showing high expression (EGFP+/mCherry+) and minimal expression (EGFP−/mCherry−) were collected (squares). Indexes of numbers and percentages of collected cells are listed in Table S5 in Supporting Information. Vertical and horizontal lines indicate background fluorescence levels of EGFP and mCherry, respectively. (C) Cel-I assays of cells transfected with the *HPRT1_B* and *HPRT1*_E TALEN-encoding separate vectors (Ligation−) and single vectors (Ligation+). The arrowheads indicate the expected positions of the digested products.% NHEJ (nonhomologous end-joining) was estimated using ImageJ software as previously described (Hansen *et al.* 2012). (D) Genomic RCR analysis of chromosomal deletions at the *HPRT1* locus of unselected, EGFP−/mCherry−, and EGFP+/mCherry+ cells transfected with the *HPRT1*_B and *HPRT1*_E TALEN-encoding plasmids and untransfected control cells. The arrowhead indicates the expected position of the PCR product with the 1100-bp deleted sequence. (E, F) Frequencies of chromosomal deletions in unselected (E) and EGFP+/mCherry+ (F) cells. The genomic PCR products were subcloned, and colony PCR was carried out. After analysis by agarose gel electrophoresis, the nucleotide sequences of the smaller DNA fragments were determined. Red clone numbers indicate the sequenced clones. The wild-type sequence of *HPRT1* is shown at the top with the TALEN target sequence (capital letters with underlines). Deletions are indicated by dashes.

expression vectors using the mismatch-sensitive endonuclease (Cel-I) assay (Fig. 4C). The results showed that the mutagenic frequencies of the unified TALEN vectors were at similar levels to those of the separate TALEN expression vectors.

To enrich cells with large deletions, we simultaneously transfected the unified expression vectors for the *HPRT1*_B and *HPRT1*_E TALEN pair-expressing plasmids into HCT116 cells. At 72 h post-transfection, we obtained unselected, EGFP−/mCherry− and EGFP+/mCherry+ cells and amplified the DNA fragments including the *HPRT1*_B and *HPRT1*_E TALEN target sites by PCR using genomic DNA extracted from these cells as well as negative control cells (Fig. 4B, squares; Fig. 4D). We clearly observed 1100-bp deleted DNA fragments in the PCR products of EGFP+/mCherry+ cells and weakly detected such fragments in the products of transfected-unselected cells, but did not detect such fragments in the products of untransfected-unselected cells and EGFP−/mCherry− cells. To investigate whether the smaller DNA fragments were caused by chromosomal deletions, the DNA fragments amplified by PCR using genomic DNA extracted from unselected cells were subcloned, and the nucleotide sequences of the smaller DNA fragments were determined (Fig. 4E). As a result, we found that the left site of the *HPRT1*_E TALENs and right site of the *HPRT1*_B TALENs were joined and that a region of approximately 1100 bp in length of the genomic sequence between the two TALEN sites was deleted. The frequency of chromosomal deletions was 3% in unselected cells. In addition, large deletions were observed in the DNA fragments of EGFP+/mCherry+ cells by sequencing, and the frequency of these large deletions was 41%, showing 13.7-fold enrichment of deleted cells after the selection (Fig. 4F).

Next, we investigated whether this system enables the enrichment of cells with large deletions in an autosomal genomic locus. We constructed two pairs of TALENs targeting the *ATM* locus using the FUSE method, in which the *ATM*_A TALEN target site was located approximately 1400-bp downstream of the *ATM*_D TALEN target site (Fig. 5A). After confirmation of the TALEN activities by the SSA assay, we examined the formation of short indels (Fig. 5C) and large deletions (Fig. 5D) with or without fluorescence selection (Fig. 5B). We subsequently analyzed the deletion frequencies in transfected cells by DNA sequencing. For the *ATM* locus, the frequencies of chromosomal deletions were 11% (Fig. 5E) and 77% (Fig. 5F) in unselected and EGFP+/mCherry+ cells, respectively, indicating 7-fold enrichment of cells with large deletions after the selection (Table 1).

Enrichment of cells with TALEN-induced extra-large chromosomal deletions

To test the ability of our FUSE method and FAST-id system to enrich cells with more complex chromosomal rearrangements, we finally tried enrichment of cells with extra-large chromosomal deletions, chromosomal inversions and translocations. We additionally constructed a pair of TALEN targeting nuclear protein, ataxia–telangiectasia locus (*NPAT*) gene (*NPAT*_A TALEN, Fig. 6A), whose target site is approximately 30 kb away from *ATM*_A TALEN target site. After confirming the mutagenic activity of FUSEd and unFUSEd *NPAT*_A TALENs by Cel-I assay (Fig. 6C), we transfected *NPAT*_A and *ATM*_A TALEN

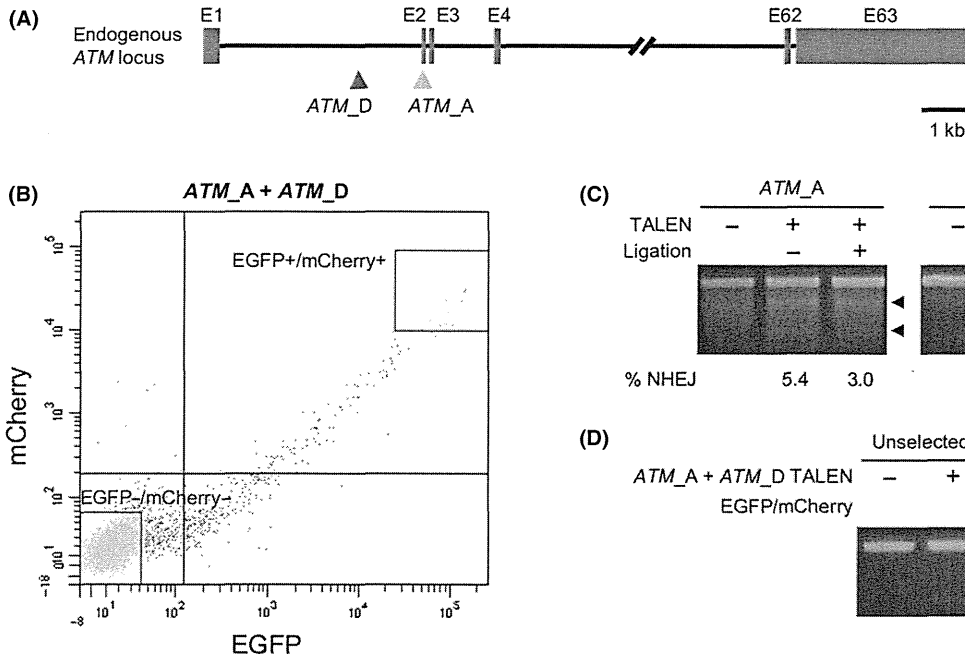

(E) *ATM*_A + *ATM*_D TALEN (Unselected cells)

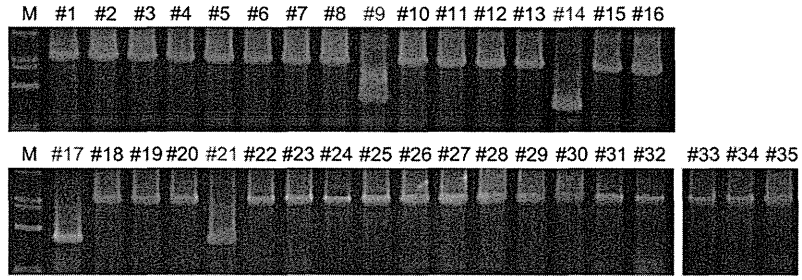

ATM_A + ATM_D Unselected cells 11%(4/35)

*ATM*_D TALEN Left site — *ATM*_A TALEN Right site

```
gaggcttggtGTACGAATGATCCTGTCactcaggtagtgagc..1390bp..tgcttatctgctgccGTCAACTAGAACATGATagagctacag WT
gaggcttggtGTACGAATGATCCTGTCacgg----------tgccGTCAACTAGAACATGATagagctacag x2
gaggcttggtGTACGAATGATCCTGTCac----------tgccGTCAACTAGAACATGATagagctacag x2
```

(F) *ATM*_A + *ATM*_D TALEN (EGFP+/mCherry+ cells)

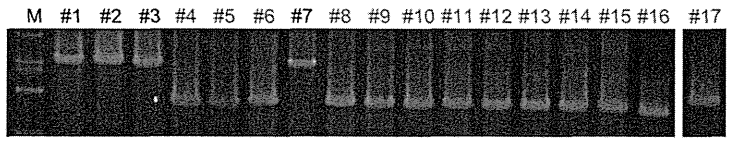

ATM_A + ATM_D EGFP+/mCherry+ cells 77%(13/17)

*ATM*_D TALEN Left site — *ATM*_A TALEN Right site

```
gaggcttggtGTACGAATGATCCTGTCactcaggtagtgagc..1390bp..tgcttatctgctgccGTCAACTAGAACATGATagagctacag WT
gag----------ctacag x2
gaggcttggtGTACGAATGATCCTGTCactcaggttag----------tgctgccGTCAACTAGAACATGATagagctacag
gaggcttggtGTACGAATGATCCTGTCactctgct----------gccGTCAACTAGAACATGATagagctacag
gaggcttggtGTACGAATGATCCTGTCactcag----------ccGTCAACTAGAACATGATagagctacag
gaggcttggtG-------GATCaT----------ctgccGTCAACTAGAACATGATagagctacag
gaggcttggtGTACGAATGATCCTGTCactcaggttg----------gctgccGTCAACTAGAACATGATagagctacag
gaggcttggtGTACGAATGATCCTGTCactc----------tgccGTCAACTAGAACATGATagagctacag
gaggcttggtGTACGAATGATCCTGTCactcagg----------cGTCAACTAGAACATGATagagctacag
gaggcttggtGTACGAATGATCCTGTCa----------tgccGTCAACTAGAACATGATagagctacag
gaggcttggtGTACGAATGATCCTGTCactcaggtagt----------ctgccGTCAACTAGAACATGATagagctacag
gaggcttggtGTACGAATGATCCTGTCactcaggtagt----------AACTAGAACATGATagagctacag
gaggcttggtGTACGAATGATCCTGTCactcaggtaat----------gctgccGTCAACTAGAACATGATagagctacag
```

Figure 5 Enrichment of chromosomally deleted cells at the *ATM* locus. (A) Schematic illustration of the human *ATM* gene. The target sites of the *ATM*_A and *ATM*_D TALENs are shown by the yellow and red arrowheads, respectively. E, exon. (B) Flow cytometric analysis of HCT116 cells transfected with the *ATM*_A and *ATM*_D TALEN-encoding plasmids. Cells showing high expression (EGFP+/mCherry+) and minimal expression (EGFP−/mCherry−) were collected (squares). Indexes of numbers and percentages of collected cells are listed in Table S5 in Supporting Information. Vertical and horizontal lines indicate background fluorescence levels of EGFP and mCherry, respectively. (C) Cel-I assays of cells transfected with the *ATM*_A and *ATM*_D TALEN-encoding separate vectors (Ligation−) and single vectors (Ligation+). The arrowheads indicate the expected positions of the digested products.% NHEJ (nonhomologous end-joining) was estimated using ImageJ software as previously described (Hansen *et al.* 2012). (D) Genomic RCR analysis of chromosomal deletions at the *ATM* locus of unselected, EGFP−/mCherry−, or EGFP+/mCherry+ cells transfected with the *ATM*_A and *ATM*_D TALEN-encoding plasmids and untransfected control cells. The arrowhead indicates the expected position of the PCR product with the 1400-bp deleted sequence. (E, F) Frequencies of chromosomal deletions in unselected (E) and EGFP+/mCherry+ (F) cells. The genomic PCR products were subcloned and colony PCR was carried out. After analysis by agarose gel electrophoresis, the nucleotide sequences of the smaller DNA fragments were determined. Red clone numbers indicate the sequenced clones. The wild-type sequence of *ATM* is shown at the top with the TALEN target sequence (capital letters with underlines). Deletions are indicated by dashes.

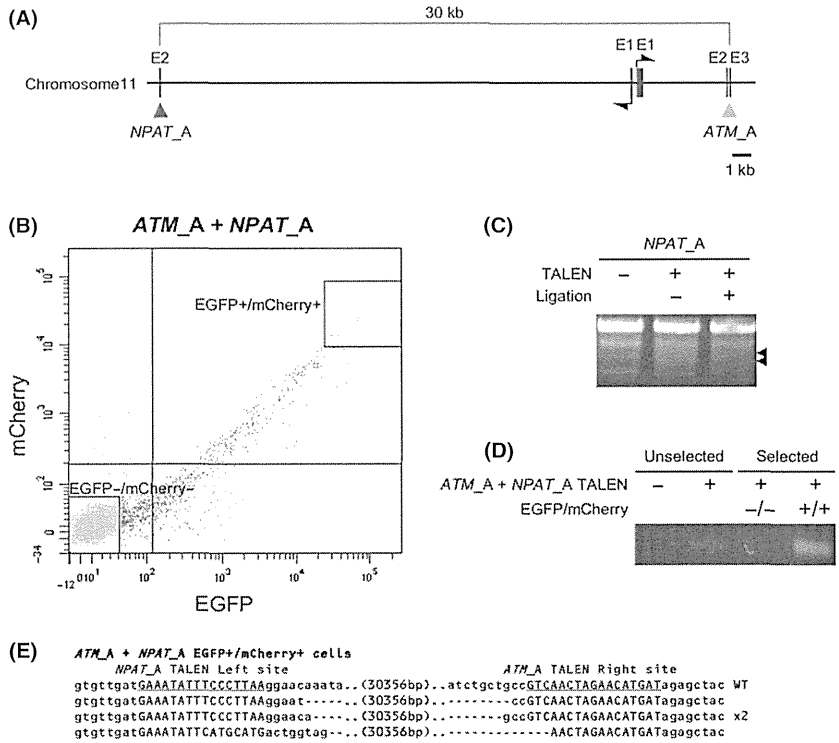

Figure 6 Enrichment of cells with extra-large chromosomal deletions. (A) Schematic illustration of a part of human chromosome 11. The target sites of *ATM*_A and *NPAT*_A TALENs are shown by the yellow and red arrowheads, respectively. E, exon. (B) Flow cytometric analysis of HCT116 cells transfected with *ATM*_A and *NPAT*_A TALEN-encoding plasmids. Cells showing high expression (EGFP+/mCherry+) and minimal expression (EGFP−/mCherry−) were collected (squares). Indexes of numbers and percentages of collected cells are listed in Table S5 in Supporting Information. Vertical and horizontal lines indicate background fluorescence levels of EGFP and mCherry, respectively. (C) Cel-I assay of the cells transfected with *NPAT*_A TALEN-encoding separate vectors (Ligation-) and a single vector (Ligation+). The arrowheads indicate the expected positions of the digested products. (D) Genomic RCR analysis of extra chromosomal deletions at the chromosome 11 of unselected, EGFP−/mCherry−, or EGFP+/mCherry+ cells transfected with *ATM*_A and *NPAT*_A TALEN-encoding plasmids and untransfected control cells. (E) Sequences observed in EGFP+/mCherry+ cells transfected with *ATM*_A and *NPAT*_A TALEN-encoding plasmids. The wild-type sequence of a part of chromosome 11 is shown at the top with the TALEN target sequence (capital letters with underlines). Deletions are indicated by dashes.

pair-expressing plasmids into HCT116 cells. Genomic PCR and DNA sequencing showed that cells with 30-kb chromosomal deletions were successfully enriched by FACS selection (Fig. 6B,D,E).

It has been reported that chromosomal inversion sometimes occurs with the use of two pairs of TALENs targeting the same chromosome (Lee *et al.* 2012; Gupta *et al.* 2013; Xiao *et al.* 2013). Therefore, we carried out PCR analyses to investigate whether chromosomal inversions were generated. For *HPRT1*, one of the ten sequences (Fig. 4F, #7 among the black-lettered numbers) exhibited chromosomal inversion with an expected size in EGFP+/mCherry+ cells transfected with the *HPRT1*_B and *HPRT1*_E TALEN pair expression vectors. However, no chromosomal inversions were detected in 35 sequences (Fig. 4E, all black-lettered numbers) with the expected size in unselected cells transfected with the *HPRT1*_B and *HPRT1*_E TALEN expression vectors. On the other hand, chromosomal inversions were not detected in cells transfected with the *ATM*_A and *ATM*_D TALEN expression vectors.

Double-strand breaks induced on different chromosomes potentially cause chromosomal translocations (Brunet *et al.* 2009; Piganeau *et al.* 2013). We transfected *ATM*_A and *HPRT1*_E TALEN pair-expressing plasmids into HCT116 cells, collected EGFP+/mCherry+ cells, and tried to detect translocated alleles by genomic PCR analysis, but no intended amplicons appeared.

Discussion

In this study, we have showed that our FAST-id system enabled enrichment of cells with TALEN-induced mutations and that the combination of the FAST-id system and FUSE method efficiently enriched cells with TALEN-induced large deletions.

The FAST-id system and FUSE method have several advantages compared with conventional methods using additional reporter vectors. First, we construct a bicistronic expression vector that is expected to express the same number of TALEN and fluorescent protein molecules, meaning that there is no necessity to construct and transfect additional plasmids. Furthermore, transfection of the vector enables us to exactly identify the cells expressing the TALEN and evaluate the expression level of the TALEN by monitoring the expression level of the fluorescent protein. Second, the FUSE method enables us to construct vectors that express the same molecular number of left TALEN, right TALEN, and fluorescent protein, and thus, the combination of the FAST-id system and FUSE method enables us to select cells expressing both the left and right TALENs by monitoring the fluorescent protein. Third, our system enables us to reduce the kinds of vectors required for transfection, which is expected to improve the selection efficiency for cells with mutations. In fact, the mutation rates of TALEN-transfected cells after selection in this study (83% and 100%) were higher than those in previous studies (Kim *et al.* 2011, 2013a). Moreover, our methods are thought to be capable of enriching cells with TALEN-induced mutations and large deletions after synthesized mRNA transfection, whereas DNA transfection, which has a risk of random integration into the genome, is indispensable for previous reporter vector-based methods. Fourth, our system is easy to use, because the novel vectors for the FAST-id system and FUSE method are fully compatible with the Golden Gate TALEN and TAL Effector Kit (Cermak *et al.* 2011) and the Yamamoto Laboratory TALEN Construction and Evaluation Accessory Pack (Sakuma *et al.* 2013) distributed by Addgene (Cambridge, MA, USA).

Transcription activator-like effector nuclease-mediated large deletion is a useful technique for analyzing the functions of not only a single gene, but also multiple genes. In zebrafish, it has been reported that a noncoding RNA gene cluster was successfully excised from the genome using two pairs of TALENs (Liu *et al.* 2013). In that case, the excised genomic region was approximately 1.2 kb in length, which was a similar size to the experiments in the present study. Furthermore, it has been shown that much larger genomic regions, up to megabases in length, can be deleted through the use of two pairs of TALENs in zebrafish (Gupta *et al.* 2013) and cultured cells (Kim *et al.* 2013b). Although a previous report estimated quite low frequencies of TALEN-mediated large chromosomal deletions (0.61% for 3.6-Mb deletion and 0.40% for 24-Mb deletion; Kim *et al.* 2013b), our FAST-id system and FUSE method have the possibility of enriching cells with such large chromosomal deletions, thereby enabling the disruption of multiple genes including clustered genes that have redundant functions and disease-related genes that are known to cause afflictions such as cancer and neuropsychiatric disorders through copy number variations.

As all the TALENs used in this study contain homodimeric FokI nuclease domains, there remains to be improved regarding targeting specificity. It is expected that TALENs containing obligate heterodimeric FokI nuclease domains will significantly

decrease the risk of off-target mutations, especially in the experiments using two pairs of TALENs.

In conclusion, our system is simple, easy, and reliable for the enrichment of cells with TALEN-induced mutations or large deletions. To the best of our knowledge, this is the first report of efficient enrichment of cells with TALEN-induced chromosomal deletions. Importantly, we successfully showed not only approximately 1-kb deletions but also 30-kb extra-large chromosomal deletions. Our system will promote the utility of TALENs in both basic and biomedical research.

Experimental procedures

Construction of co-expression vectors for TALENs and fluorescent proteins

The pcDNA-mC-2A-TAL-NC2 plasmid, a destination vector for construction of the mCherry-2A-TALEN expression plasmid, was constructed by the In-Fusion cloning method (Clontech, Mountain View, CA, USA). Briefly, the mCherry sequence was amplified by PCR using mCherry-F and mCherry-2A-R primers (Table S1 in Supporting Information). 2A sequences were synthesized and converted to double-stranded DNA by primer extension using 2A-F and 2A-R oligonucleotides (Table S1 in Supporting Information). pcDNA-TAL-NC2 plasmids (Addgene) were linearized by inverse PCR using pcDNA-TAL-NC-Inverse-F and pcDNA-TAL-NC-Inverse-R primers (Table S1 in Supporting Information). These three DNA fragments were assembled by the In-Fusion cloning method. As the products generated by In-Fusion cloning erroneously contained a stop codon in the mCherry sequence, it was excluded by inverse PCR using 2A-Inverse-F and mCherry-Inverse-R primers (Table S1 in Supporting Information) to generate pcDNA-mC-2A-TAL-NC2 plasmids. The pcDNA-eG-2A-TAL-NC2 plasmid, a destination vector for construction of the EGFP-2A-TALEN expression plasmid, was constructed by the In-Fusion cloning method. Briefly, pcDNA-mC-2A-TAL-NC2 plasmids were linearized, and the mCherry sequence was excluded using pcDNA-TAL-NC-2A-Inverse-F and pcDNA-TAL-NC-Inverse-R primers (Table S1 in Supporting Information). The EGFP sequence was amplified by PCR using Infusion-EGFP-F and Infusion-EGFP-R primers (Table S1 in Supporting Information). These two DNA fragments were assembled by the In-Fusion cloning method. For unification of one TALEN pair into a single vector, pcDNA-mC-2A-TAL-NC2-Uni, pcDNA-eG-2A-TAL-NC2-Uni, and pcDNA-2A-TAL-NC2-Uni plasmids were constructed as destination vectors for construction of mCherry-2A-TALEN-(BamHI), EGFP-2A-TALEN-(BamHI), and (BamHI)-2A-TALEN expression vectors, respectively. The pcDNA-mC-2A-TAL-NC2-Uni and pcDNA-eG-2A-TAL-NC2-Uni plasmids were constructed by inverse PCR using +BamHI-FokI-F and +BamHI-FokI-R primers (Table S1 in Supporting Information) for insertion of a BamHI site (5′-GGATCC-3′). The pcDNA-2A-TAL-NC2-Uni plasmid was constructed by inverse PCR from the pcDNA-mC-2A-TAL-NC2 plasmid using +ATG + BamHI-2A-F and pcDNA-TAL-NC-Inverse-R primers (Table S1 in Supporting Information) to exclude the mCherry sequence and insert a start codon and BamHI site (5′-ATGGGATCC-3′).

Design and construction of TALENs

The design of the *HPRT1*_B TALENs was described previously (Sakuma *et al.* 2013). *HPRT1*_E, *ATM*_A, and *ATM*_D TALENs were newly designed using TAL Effector Nucleotide Targeter 2.0 (Doyle *et al.* 2012; https://tale-nt.cac.cornell.edu/node/add/talen-old). The target sites of each TALEN are listed in Table S2, in Supporting Information (capital letters). The TALENs were constructed as previously described (Sakuma *et al.* 2013) using the modified destination vectors described above. The combinations of the TALEN arrays and vectors used are listed in Table S3 in Supporting Information. The left and right TALEN arrays of one TALEN pair were unified into a single vector by double restriction enzyme digestion using BamHI (Takara Bio, Shiga, Japan) and PvuI (TaKaRa Bio) and subsequent ligation. Successful construction of one TALEN pair into a single vector was confirmed by digestion with XbaI (Takara Bio). Because the vector contained XbaI sites exclusively in the N-terminal domains of the TALENs, an approximately 3-kb DNA fragment appeared after XbaI digestion if the two TALEN vectors were assembled successfully.

Transfection and Cel-I assay

Transfection for the Cel-I assay was carried out as follows. On the day before transfection, 200 000 HCT116 cells were plated into 35-mm dishes. On the day of transfection, a total of 2.5 μg of TALEN plasmids was transfected using 5.0 μL of Lipofectamine LTX (Invitrogen, Carlsbad, CA, USA) and 2.0 μL of Plus Reagent (Invitrogen) according to the manufacturer's instructions. On the day after transfection, the cells were moved to 60-mm dishes. At 72 h post-transfection, the cells were collected and their genomic DNA was isolated using a DNeasy Blood & Tissue Kit (Qiagen, Hilden, Germany). Genomic PCR was carried out with the primers listed in Table S4 in Supporting Information. The amplified products were purified with a Wizard SV Gel and PCR Clean-Up System (Promega, Madison, WI, USA), and 400 ng of purified DNA was used for the Cel-I assay with a SURVEYOR Mutation Detection Kit (Transgenomic, Omaha, NE, USA) according to the manufacturer's instructions. The products were analyzed by electrophoresis in 3% agarose gels and ethidium bromide staining.

Transfection and FACS

Transfection for cell sorting was carried out as described above with several modifications. On the day before transfection,

REVIEW

Hepatoblastoma state of the art: pathology, genetics, risk stratification, and chemotherapy

Piotr Czauderna[a], *Dolores Lopez-Terrada*[b], *Eiso Hiyama*[c], *Beate Häberle*[d], *Marcio H. Malogolowkin*[e], *and Rebecka L. Meyers*[f]

Purpose of review
As a rare pediatric tumor, hepatoblastoma presents challenges to the individual practitioner as no center will see more than a handful of cases each year.

Recent findings
The Children's Hepatic tumor International Collaborative (CHIC) effort has fostered international cooperation in this rare children's tumor, leading to the establishment of a large international collaborative dataset, the CHIC database, which has been interrogated to refine risk stratification and inform treatment options. Apace with this effort has been the international collaboration of pediatric pathologists working together to establish a new international histopathologic consensus classification for pediatric liver tumors as a whole, with particular focus on the histological subtypes of hepatoblastoma.

Summary
International collaborative efforts in hepatoblastoma have led to a new international histopathologic consensus classification, refinements in risk stratification, advances in chemotherapy, and a better understanding of surgical resection options forming the foundation for the development of an upcoming international therapeutic trial.

Keywords
chemotherapy, genetics, hepatoblastoma, pathology, risk stratification

INTRODUCTION

This is part one of a two-part state of the art – hepatoblastoma. The companion, part two, article deals with *PRE-T*reatment *EXT*ent of tumor (PRETEXT) radiographic staging, surgical guidelines and liver transplantation and also appears in this issue. Over the last 4 decades, overall survival in hepatoblastoma has increased from roughly 30% to over 80%, primarily because of advances in chemotherapy and in our ability to achieve complete surgical resection, even in the most advanced of tumors. Detailed herein are some of the key advances in histopathology, epidemiology, genetics, chemotherapy, and risk stratification that have helped drive the improved survival seen in hepatoblastoma.

HISTOPATHOLOGY AND EPIDEMIOLOGY OF HEPATOBLASTOMA

Although primary liver tumors are rare in children, hepatoblastoma is the most common primary pediatric liver tumor, usually diagnosed during the first 3 years of life [1]. Most cases of hepatoblastoma are sporadic; however, some are associated with constitutional genetic abnormalities, malformations, and familial cancer syndromes, such as Beckwith–Wiedemann syndrome (BWS) and familial adenomatous polyposis (FAP) [2–4]. Recent pediatric cancer epidemiological studies, including the US National Cancer Institute Surveillance Epidemiology and End Results (SEER), as well as others in Japan and Europe [5,6], report an average

[a]Department of Surgery and Urology for Children and Adolescents, Medical University of Gdansk, Gdansk, Poland, [b]Department of Pathology, Texas Children's Hospital and Baylor College of Medicine, Houston, Texas, USA, [c]Department of Surgery, Natural Science Center for Basic Research and Development, Hiroshima University Hospital, Hiroshima, Japan, [d]Children's Hospital, Ludwig-Maximilians-University, Munich, Germany, [e]Department of Pediatric Hematology and Oncology, Children's Hospital of Wisconsin, Milwaukee, Wisconsin and [f]Department of Pediatric Surgery, Primary Children's Medical Center, University of Utah, Salt Lake City, Utah, USA

Correspondence to Rebecka L. Meyers, MD, Professor of Pediatric Surgery, University of Utah, Pediatric Surgery Suite 2600, Primary Children's Medical Center, 100 Mario Capecchi Drive, Salt Lake City, UT 84103, USA. Tel: +1 801 662 2950; e-mail: rebecka.meyers@imail.org

Curr Opin Pediatr 2014, 26:19–28
DOI:10.1097/MOP.0000000000000046

KEY POINTS

- New international pediatric hepatoblastoma consensus classification (Table 1) includes histological subtypes and categories, recognizing how challenging some tumors are to classify, particularly after chemotherapy.
- CHIC risk factor analysis (Table 3) shows refined prognostic estimates in smaller subgroups than previously possible by interrogating a collaborative dataset that includes comprehensive data on 1605 children treated by the four major hepatoblastoma study groups between 1989 and 2008.
- SIOPEL 4 shows an impressive improvement in survival for metastatic patients using a novel schema that incorporated weekly dose-dense cisplatin chemotherapy (Table 6).
- COG, SIOPEL/GPOH, and JPLT are now collaborating to develop a cooperative international hepatoblastoma trial, fostering our ability to compare the historic differences between the chemotherapeutic and surgical approaches of different study groups and enhance biologic study in this rare tumor.

annual percentage increase in the incidence of hepatoblastoma during the last 30 years. Indeed, the incidence does seem to be slowly increasing, with a current rate of 1.2–1.5 cases/million population/year. Because premature birth and very low birth weight have been found to be associated with the later appearance of hepatoblastoma, increase in these patient cohorts may be driving the increase in incidence [7▪]. Oxygen therapy, medications such as furosemide, Total Parenteral Nutrition (TPN), radiation, plasticizers, and other toxins are postulated to perhaps play a role, but the exact mechanisms are not yet understood.

Hepatoblastoma is an embryonal tumor thought to originate from a hepatocyte precursor cell (hepatoblast) that often recapitulates the stages of liver development, displaying a combination of histological patterns [8]. Clinical trials have demonstrated that, in addition to staging, some histological types are also associated with prognosis [9]. One early review showed that 67% of hepatoblastomas were epithelial, with a combination of mixed embryonal and fetal patterns, and 21% displayed a mesenchymal component in addition to the common epithelial patterns. Most importantly, approximately 7% of the total were composed of a pure, well differentiated fetal (WDF) epithelial component, and 5% demonstrated primitive appearing or so-called small cell undifferentiated (SCU) tumor cells [10]. Since then, several studies have demonstrated a correlation between improved survival and WDF histology composed only of cells resembling fetal hepatocytes with minimal mitotic activity. In a recent Children's Oncology Group (COG) publication, Malogolowkin *et al.* [11] reported that, whenever complete tumor specimens can be resected and evaluated prior to chemotherapy, patients with WDF histology [formerly referred to as pure fetal histology (PFH)] and low mitotic activity may be treated exclusively with surgery, and no chemotherapy is necessary. Patients with WDF/PFH histology completely resected upfront and receiving no postoperative chemotherapy comprised 7% of the total number of patients (COG studies INT-0098 and P9645) and showed 100% event-free survival (EFS). This is in striking contrast to other international protocols, which historically have treated all children with liver tumors and elevated alphafetoprotein (AFP) with chemotherapy prior to surgical resection [12▪▪]. It is important to remember, though, that most hepatoblastomas are extremely heterogeneous, often with closely intermixed histological components, and only rarely composed of a single histological type [13▪▪].

A second histological subtype worth mentioning is the SCU. This may be part of an otherwise typical hepatoblastoma, representing a component intermixed with other histologies or present as the sole component in the so-called 'pure small cell' hepatoblastoma. This histologic pattern is sometimes associated with low serum AFP levels and poor response to chemotherapy. The first report regarding the negative association of SCU component was by Kasai and Watanabe, followed by Haas's Children's Cancer Group–Pediatric Oncology Group (CCG–POG, also referred to as COG legacy groups) report, in which none of the patients with small cell hepatoblastoma survived 24 months after the diagnosis [14,15]. Trobaugh-Lotrario *et al.* [16] recently reviewed a large series of hepatoblastoma with small cell histology and confirmed 11 patients with SCU hepatoblastomas presenting with clinically normal or minimally increased serum AFP levels, none of whom survived. Interestingly, six of these tumors were *INI1* nuclear negative by immunohistochemical staining and three of them demonstrated cytogenetic and molecular abnormalities similar to those seen in rhabdoid tumors, suggesting that some, but not all, of these tumors may represent *INI1*-negative neoplasms within the spectrum of primary rhabdoid tumors. However, the significance of small cell component when admixed with other epithelial types, and whether these small foci are sometimes *INI1* expressing, is still under investigation. Participants in the Los Angeles 2011 International Pathology Pediatric Liver Symposium agreed upon a panel of immunohistochemical stains

including *INI1*, which should be closely correlated with the morphology in order to further characterize this pattern and its prognostic significance. In addition, the group recommended that all *INI1*-negative tumors should be submitted for molecular testing, and patients and family members referred to a genetic counselor to possibly be screened for germline mutations whenever appropriate [13▪▪].

The rarity of hepatoblastoma, combined with the rarity of upfront resection, has resulted in a paucity of complete annotated prechemotherapy specimens, compromising biology studies. Therefore, several international conferences have been sponsored to foster international collaboration and clinical trials. As a result of these meetings, recommendations were outlined for submission, sampling, and evaluation of pediatric liver tumor samples, including minimum diagnostic specimen requirements and evaluation of the uninvolved liver, as well as the necessity of providing minimal clinical information to the reviewer, which should always include age, AFP level at the time of diagnosis, underlying liver disease, and correlation with imaging [13▪▪]. There was also consensus between the pathologists regarding the importance of obtaining prechemotherapy specimens for the initial diagnoses and tumor classification. Finally, the group also highlighted the importance of tissue banking for biological studies [13▪▪].

The newly proposed pathology consensus of pediatric hepatoblastoma classification (Table 1) [13▪▪] includes all prognostically relevant histological types (WDF and SCU), as well as the new categories ('pleomorphic epithelial' and 'malignant hepatocellular neoplasm'), recognizing how challenging some tumors are to classify, particularly after chemotherapy. Reviewers also highlighted the importance of appropriately sampling and following specimen submission recommendations, as well as the imperative need to characterize the biology of hepatoblastoma, pediatric hepatocellular carcinoma, and other hepatocellular neoplasms, and to identify biological markers that could be used for tumor classification, clinical stratification, and to develop new novel therapeutic strategies.

Table 1. International consensus classification of the histologic subtypes of hepatoblastoma

Epithelial	Subtype/definition	Mixed	Subtype/definition
Fetal	Well differentiated and uniform (10–20 μm diameter), round nuclei, cords with minimal mitotic activity, EMH	Stromal derivatives	Spindle cells (blastema), osteoid, skeletal muscle, cartilage
	Crowded or mitotically active (>2 per 10 400× microscopic fields); conspicuous nucleoli (usually less glycogen)	Teratoid	Mixed, plus primitive endoderm; neural derivatives, melanin, squamous and glandular elements
	Pleomorphic, poorly differentiated Moderate anisonucleosis, high N/C, nucleoli		
	Anaplastic with marked nuclear enlargement and pleomorphism, hyperchromasia, abnormal mitoses		
Embryonal	10–15 μm diameter, high N/C, angular, primitive tubules, EMH		
Macrotrabecular	Epithelial HB (fetal or embryonal) growing in clusters of >5 cells between sinusoids		
Small cell undifferentiated (SCU)	(5–10 μm diameter) no architectural pattern, minimal pale amphophilic cytoplasm, round to oval nuclei with fine chromatin and inconspicuous nucleoli, +/- mitoses; +/- INI[a]		
Cholangioblastic	Bile ducts, usually at periphery of epithelial islands, can predominate		

EMH, extramedullary hematopoiesis; HB, hepatoblastoma. Data from [13▪▪]

[a]Pure small cell undifferentiated needs to be differentiated from malignant rhabdoid tumors (discohesive, eccentric irregular nuclei, prominent nucleoli, abundant cytoplasmic filaments including cytokeratin and vimentin, negative nuclear INI).

PREDICTING PROGNOSIS: GENETICS

Several prognostic markers and constitutional genetic syndromes such as Trisomy 18/Edward's syndrome, BWS, and FAP have been reported in association with hepatoblastoma [17]. There have been at least seven published cases of hepatoblastoma in children with trisomy 18/Edward's syndrome. BWS predisposes to a number of embryonal tumors and the overall percentage of children with BWS who develop tumors is 7.5–13.5%, with the most frequent tumors being Wilms' tumor and hepatoblastoma. Regarding FAP, it appears that there may be genotype–phenotype links between specific mutations to the *APC* gene, which is mutated in FAP. In families with FAP and hepatoblastoma, referral to a genetic counselor is recommended.

The most frequent genetic aberrations (70–90%) in hepatoblastoma occur in genes involved in the *Wnt* signaling pathway [18,19]. A majority of hepatoblastoma have *Wnt* signal abnormalities. Recently, telomerase activation and genetic expression profiles were identified as prognostic factors [20,21]. Among 212 hepatoblastoma enrolled in Japanese Study Group for Pediatric Liver Tumors (JPLT)-2 between 2000 and 2010, large deletion of *CTNNB1* was detected in 107 cases and mutation of *CTNNB1* exon 3 was detected in 56 cases. Approximately 80% had abnormalities of these factors, including *APC* and *Axin* genes. Immunohistochemistry revealed β-catenin was accumulated in the tumor cells with *Wnt* signal aberrations. Not all, but a majority, of the samples showed elevated expression of *Wnt* signal target genes such as *cyclin D1*, *survivin*, and *MYC*.

Telomerase, the activated enzyme related to cell immortality, is a reverse transcriptase for the elongation of telomeres, is regulated by the expression of *TERT* (human telomerase reverse transcriptase), and is a catalytic component of human telomerase [22,23]. *Wnt* signal activation usually occurs in aggressive tumors, *TERT* expression plays a major role in *Wnt* signal activation, and *MYC* (an activated *Wnt* signal target gene) enhances *TERT* expression. As a result, activation of *TERT* and *MYC* signaling appears to play a role in the more aggressive phenotypes of hepatoblastoma [24,25]. Additionally, recent microarray analysis by Cairo and colleagues revealed a 16-gene signature that discriminated invasive and metastatic hepatoblastoma and predicted prognosis. These 16 genes were the highly proliferating subclass typified by upregulated *MYC* signaling [26]. These findings support the *MYC* activation theory by *Wnt* signaling activation in aggressive hepatoblastoma, again suggesting that a *TERT* and *MYC* vicious cycle may exist in aggressive tumors.

PREDICTING PROGNOSIS: RISK STRATIFICATION AND CLINICAL PROGNOSTIC FACTORS

The four major study groups – International childhood liver tumors strategy group (SIOPEL), COG, German Society for Pediatric Oncology (GPOH), and JPLT – have historically had disparate risk classification categories, making it difficult to compare the outcomes across the oceans. Fortunately, all groups have increasingly used the PRETEXT grouping system for risk stratification, as discussed in Part Two of this review. Over the last 10 years, individual study groups have attempted to define the relative importance of a variety of suspected prognostic factors present at diagnosis and in response to therapy [9,11,27,28,29▪▪,30] (Table 2). In SIOPEL, good prognostic factors have included low PRETEXT at diagnosis (PRETEXT I, II, and III tumors) [28]. In COG, good prognosis has been shown for Stage I tumors resected at diagnosis and tumors with pure fetal histology [9,11]. Poor prognostic factors identified individually in these trials include PRETEXT IV, metastatic disease, AFP less than 100, and SCU histology [9,27]. Other variables such as tumor rupture prior to diagnosis, tumor multifocality, macrovascular tumor invasion, extrahepatic tumor extension, age at diagnosis, very high (>1.2 million) or borderline low (100–1000) AFP have been

Table 2. Potential prognostic factors in hepatoblastoma

Pre-treatment	Response to treatment
PRETEXT (I[a], II[a], III, IV[d])	Response to chemotherapy
Metastasis at diagnosis[b]	Positive surgical margins
Unresectable vessel involvement (+V, +P)[b]	Surgical resectability
Extrahepatic tumor extension (+E)[b]	Tumor relapse
Lymph nodes	
Multifocal tumor[b]	
Tumor rupture at diagnosis[b]	
AFP level (<100[b]; 100–1000[b]; >1 million)	
Pathologic subtype (pure fetal[c], small cell undifferentiated[d])	
Age (<1 year[a]; >6 years[b])	
Birth weight	
Platelet count	
Co-morbidity	

AFP, alphafetoprotein; CHIC, Children's Hepatic tumor International Collaboration.
[a]Good prognostic factor in CHIC multivariate analysis [30].
[b]Poor prognostic factor in CHIC multivariate analysis [30].
[c]Good prognostic factor [11].
[d]Poor prognostic factor [9,28,29▪▪].

suggested as poor prognostic factors, but the relative importance of their prognostic significance has been difficult to define [29▪▪]. Factors in response to treatment that had been hypothesized as poor prognostic factors include poor response or progressive disease on chemotherapy, gross positive surgical margins, surgically unresectable tumor, and tumor relapse.

Efforts to define clinical prognosis in hepatoblastoma have historically been challenging because of the low numbers of patients, even in multicenter trials. To address this challenge, the Children's Hepatic tumor International Collaboration (CHIC) initiative was formed to combine the results of multicenter trials by SIOPEL, COG, JPLT, and GPOH over the last 20 years and thereby gain enhanced statistical power with increased numbers. In cooperation with the data management group Consorzio Interuniversitario (CINECA), CHIC created a dataset that includes comprehensive data on all children treated in 11 separate trials by the four major hepatoblastoma study groups between 1989 and 2008, a total of 1605 patients [31]. Univariate analysis was used to identify statistically significant prognostic variables, which were then included in a backwards elimination multivariate analysis to identify those constellations of variables most predictive of outcome [30]. Factors significant by univariate analysis at diagnosis were PRETEXT, AFP less than 100, AFP 100–1000, metastatic disease, age group, macrovascular involvement vena cava/hepatic veins (+V), macrovascular involvement portal veins (+P), contiguous extrahepatic tumor (E), multifocal disease, and spontaneous rupture at diagnosis. Multivariate analysis of these factors led to the selection of a risk backbone based upon PRETEXT I/II, PRETEXT III, PRETEXT IV, AFP less than 100, and metastatic disease. Within each of these backbone groups, the presence or absence of the remaining risk factors was further stratified by multivariate estimates of EFS (Table 3) [30]. This statistical effort is ongoing and has not yet been rigorously validated. Upon maturation of outcome data from the current COG trial, AHEP0731, the CHIC group hopes to combine the data of AHEP0731 and SIOPEL 4 to form a validation set for the CHIC risk groups. Moreover, validation and refinement of these risk groups is one of the primary objectives in the planning for an upcoming international collaborative hepatoblastoma therapeutic trial.

HEPATOBLASTOMA MULTICENTER TRIALS

Treatment of hepatoblastoma in children represents a true success story of pediatric oncology in the last 25 years. From prechemotherapy survival rates in

Table 3. Multivariate analysis of risk groups in the Children's Hepatic tumor International Collaboration (CHIC) database

PRETEXT	Age (years)	AFP	Other risk factors[a] (0, 1, ≥2)	# Patients in CHIC database[b]	5-Year EFS
I and II	<3	>100	0	375	92%
III	<1	>1000	0	125	91%
I and II	<3	>100	≥1	50	76%
I and II	3–5	>100	Any	53	74%
III	<1	>1000	≥1	43	83–86%
III	>1	>1000	0	134	87%
III	>1	>1000	1	42	74%
IV	<3	>100	0	58	77%
I and II	>6	>100	Any	28	51%
III	Any	100–1000	Any	28	61%
IV	<3	>100	1	59	66%
III	>1	>1000	>1	24	50%
IV	<3	>100	>1	32	46%
IV	>3	>100	Any	40	31%
M+ (any pretext)	Any	>100	Any and Pretext 4	259	18–48%
AFP <100 (any pretext)	Any	–	Any	65	36%

AFP, alphafetoprotein. Data from [30].
[a]Other risk factors statistically significant in multivariate analysis: multifocal tumor, major venous involvement +V (all three hepatic veins or inferior vena cava), major venous involvement +P (portal bifurcation or both portal veins), extrahepatic contiguous tumor extension +E, and tumor rupture.
[b]CHIC database includes patients from COG (INT-0098; P9645); SIOPEL (SIOPEL-2; SIOPEL-3SR, SIOPEL-3HR); JPLT (JPLT-1; JPLT-2); and GPOH (HB89; HB 99).

the 1970s of 30%, the use of adjuvant and neoadjuvant chemotherapy brought the patients' survival to 70–80%. This progress was possible not only because of the introduction of new drugs (i.e. cisplatin and doxorubicin), but also because of the new surgical approaches (i.e. hepatic exclusion, Pringle, ultrasonic dissection, liver transplantation) and, perhaps most importantly, because of multicenter cooperative efforts of the major international study groups (Table 4) [27,32–39].

One fundamental controversy between various study groups has been the issue of primary hepatic resection, with SIOPEL recommending preoperative chemotherapy in every case, in every patient, and in every tumor. The other groups have traditionally carved out some lower-risk groups amenable to upfront resection. The initial American approach (INT-0098,P9645) put the upfront surgical decision in the hands of the individual surgeon and recommended an attempt at upfront resection in everyone. The old COG Evan's stages I, II, and III were based upon the surgeon's success or failure to resect the tumor at diagnosis. In those who were not 'resectable', biopsy only was performed, followed by chemotherapy, delayed surgery, and postoperative chemotherapy. In those who were resectable, a primary partial hepatectomy was followed by postoperative chemotherapy [39]. The current COG trial, AHEP-0731, has moved away from putting surgical decisions arbitrarily in the hands of an individual surgeon. This study's surgical guidelines recommend upfront resection only for PRETEXT I and II tumors, when the diagnostic imaging shows clear radiographic margins on the contralateral portal vein, the middle hepatic vein, and the retrohepatic inferior vena cava [40].

The evolution of chemotherapeutic approaches is well illustrated by following the progression of results shown in Table 4. Contemporary chemotherapy protocols from the four major study groups

Table 4. Summary results of hepatoblastoma cooperative trials

Study	Chemotherapy	Number of patients	Outcomes
INT0098 (CCG/POG) 1989–1992	C5V vs. CDDP/DOXO	Stage: I/II: 50; Stage III: 83; Stage IV: 40	4-Year EFS/OS: I/II = 88%/100% vs. 96%/96%; III = 60%/68% vs. 68%/71%; IV = 14%/33% vs. 37%/42%
P9645 (COG) 1999–2002	C5V vs. CDDP/CARBO	Stage: I/II: pending publication; Stage III = 38; Stage IV = 50	1-Year EFS[a]: Stage III/IV: C5V 51%; CDDP/Carbo 37%
HB 94 (GPOH) 1994–1997	I/II: IFOS/CDDP/DOXO; III/IV: IFOS/CDDP/ DOXO + VP/CARBO	Stage: I: 27; II: 3; III: 25; IV: 14	4-Year EFS/OS: I = 89%/96%; II = 100%/100%; III = 68%/76%; IV = 21%/36%
HB 99 (GPOH) 1999–2004	SR: IPA; HR: CARBO/VP16	SR: 58; HR: 42	3-Year EFS/OS: SR: 90%/88%; HR: 52%/55%
SIOPEL 2 1994–1998	SR: PLADO; HR: CDDP/ CARBO/DOXO	PRETEXT: I = 6; II = 36; III = 25; IV = 21; Mets: 25	3-Year EFS/OS: SR: 73%/91%; HR: IV = 48%/61%; HR: Mets: 36%/44%
SIOPEL 3 1998–2006	SR: CDDP vs. PLADO; HR: SUPERPLADO	SR: PRETEXT I = 18; II = 133; III = 104; HR: PRETEXT IV = 74; +VPE = 70; Mets = 70; AFP <100 = 12	3-Year EFS/OS: SR: CDDP 83%/95%; PLADO 85%/93%; HR: overall 65%/69%; Mets 57%/63%
SIOPEL 4 2005–2009	HR: Block A: Weekly; CDDP/3 weekly DOXO; Block B CARBO/DOXO	PRETEXT: I = 2; II = 17; III = 27; IV = 16; Mets= 39	3-Year EFS/OS: All HR = 76%/83%; HR: IV = 75%/88%; HR: Mets: 77%/79%
JPLT 1 1991–1999	I/II: CDDP(30)/THPA-DOXO; III/IV: CDDP(60)/THPA-DOXO	Stage: I: 9; II: 32; IIIa: 48; IIIb: 25; IV: 20	5-Year EFS/OS: I = ? /100%; II = ?/76%; IIa = ?/50%; IIIb = ?/64%; IV = ?/77%
JPLT 2 1999–2010	I: low-dose CDDP Pirarubicin; II–IV: CITA Mets: High dose + stem cell transplant	Stage: *n* = 212; PRETEXT I: 95; II: 95; III: 100; IV: 48; Mets: 46	5-Year EFS/OS: I = ?/100%; II = ?/89%; III = ?/93%; IV = ?/63%; Mets 32%

AFP, alphafetoprotein; CARBO, carboplatin; CCG, Children's Cancer Group; CDDP, cisplatin; CITA, Cisplatin/Pirarubicin; COG, Children's Oncology Group; C5V, cisplatin + 5-fluorouracil (5FU) + vincristine; DOXO, doxorubicin; EFS, event-free survival; GPOH, German Society for Pediatric Oncology; HR, high risk; IFOS, ifosfamide; JPLT, Japanese Study Group for Pediatric Liver Tumors; Mets, metastatic; OS, overall survival; PLADO, cisplatin + doxorubicin; POG, Pediatric Oncology Group; PRETEXT, pre-treatment extent of tumor; SIOPEL, international childhood liver tumors strategy group; SR, standard risk; SUPERPLADO, cisplatin+ doxorubicin + carboplatin; THPA, tetrahydropyranyl adriamycin; VP, etoposide. Data from [27,32–38].
[a]Study closed early because of inferior results in CDDP/CARBO arm.

Table 5. Current chemotherapy recommendations of the different study groups

Study group	Risk group	Chemotherapy	Surgery
COG (AHEP 0731)	Very low risk	None	Primary
	Low risk	CDDP, 5FU, VCR × 2	Primary
	Intermediate risk	CDDP, 5FU, VCR, Doxo × 6–8	After 2–4 courses
	High risk	VCR, irinotecan, temsirolimus × 2	After 4–6 courses
		CDDP, 5FU, VCR, Doxo × 6	
SIOPEL (SIOPEL 6)	Standard risk	CDDP × 6	After 4 courses
(SIOPEL 4)	High risk	CDDP weekly × 8, Doxo 3rd weekly × 3	After 8 CDDP/3 Doxo
GPOH	Standard risk	CDDP, Doxo × 3–4	After 2–3 courses
	High risk	CDDP × 5 alternating CARBO/ Doxo × 5 (SIOPEL 3 HR)	After 5–7 courses
JPLT (JPLT 2)	PRETEXT I	CDDP, PIRA × 4	Primary
	PRETEXT II	CDDP, PIRA × 6	After 2 courses
	PRETEXT III/IV all V+P+E+	CDDP, PIRA × 5–6 or CDDP, PIRA × 2 + IFOS/CARBO/ PIRA/ETO × 3–4	After 3–4 courses
	All PRETEXT M+	Additional high-dose ETO/CARBO/MEL	After 4 courses

5-FU, 5-fluorouracil; CARBO, carboplatin; CDDP, cisplatin; COG, Children's Oncology Group; Doxo, doxorubicin; ETO, etoposide; GPOH, German Society for Pediatric Oncology; HR, high risk; IFOS, ifosfamide; JPLT, Japanese Study Group for Pediatric Liver Tumors; MEL, Melphalan; PIRA, pirarubicin; PRETEXT, pre-treatment extent of tumor; VCR, vincristine. Data from [12▪▪,33,38,41▪▪,42].

are shown in Table 5 [12▪▪,33,38,41▪▪,42]. The SIOPEL 1, 2, 3, 4 series of studies have shown progressive improvements in survival, especially in the high-risk (hepatoblastoma – high risk) cohorts (Table 6) [34–36,41▪▪,42]. SIOPEL 4 shows an impressive improvement in survival for metastatic patients using a novel schema that incorporated weekly dose-dense cisplatin chemotherapy. The results are startling and strike one as almost too good to be true, with 98% (60 of 61 evaluable patients) experiencing a partial response and only 1 of 20 who achieved a pulmonary complete response having relapse [43]. As a single-arm trial, SIOPEL 4 was not randomized; rather, outcomes were compared with historical controls, and therefore further study will be needed before it can be adopted as the standard of care. A total of 97% of patients had grade 3–4 hematologic toxicity. This is consistent with some adult studies that have used a similar approach and may be considered acceptable. However, fever and neutropenia occurred in 71% of patients and four patients had toxic deaths (two from infection, one from surgical bleeding, and one with tumor bleeding). The number of patients with significant hearing loss was greater than 50%. As ototoxicity is difficult to measure, notoriously underreported, and can progress over time, the question remains as to what hearing function these very young patients will have in the long run. The SIOPEL 4 results suggest that this regimen should be compared in a randomized trial, further evaluating the toxicities of this design, and, in fact, planning is underway to study this regimen in the high-risk arm of a new international trial being planned as a joint effort between COG, SIOPEL/GPOH, and JPLT. Additionally, as exciting as these results are, it

Table 6. Progression of high-risk outcomes in SIOPEL studies over the last 2 decades

	SIOPEL 1 High risk	SIOPEL 2 High risk	SIOPEL 3 High risk	SIOPEL 4 High risk
Response rate	78%	76%	77.5%	97%
Complete resection rate	58%	66%	69%	87%
EFS 3 years	45%	47%	65%	80%*
OS 3 years	57%	52%	73%	82%*
EFS metastatic	28%	44%	56%	80%*
EFS Pretext 4	46%	61%	68%	81%*

EFS, event-free survival; OS, overall survival; Pretext, pre-treatment extent of tumor; SIOPEL, international childhood liver tumors strategy group. Data from [34–36,41▪▪,42].

emphasizes the urgent need for new agents to address that subset of tumors that remain unresponsive.

Novel strategies have been investigated by JPLT and COG. In JPLT-2, the use of high-dose chemotherapy with autologous stem cell/bone marrow transplant rescue was used in the highest-risk patients, but was not found to improve survival [39]. COG AHEP-0731, in collaboration with JPLT, is studying patients using vincristine–irinotecan and vincristine–irinotecan–temsirolimus in metastatic patients in a novel upfront window design prior to beginning standard COG C5V-D chemotherapy (cisplatin, 5FU, vincristine, and doxorubicin) [44▪].

CHEMOTHERAPY, PROGRESSIVE DISEASE AND TUMOR RELAPSE: NEW DEVELOPMENTS IN CHEMOTHERAPY

Few conventional chemotherapy agents have demonstrated activity in progressive or relapse hepatoblastoma [45]. Doxorubicin, carboplatin, etoposide, and ifosfamide have been used as part of rescue strategies and have been incorporated in upfront therapy for high-risk patients as well [46–48]. Approximately one-third of the patients whose disease progressed or recurred after initial treatment without anthracyclines could be successfully rescued with a doxorubicin-containing regimen and surgery [46]. Irinotecan has been used experimentally as a maintenance therapy in a handful of patients suspected of being at high risk for relapse [47]. A SIOPEL phase 2 study investigated irinotecan in 28 patients with relapse and progressive disease on conventional chemotherapy. Of the 23 evaluable patients, 6 had a partial response, 11 had stable disease, and 6 had progressive disease. Irinotecan appeared to have significant antitumor activity in a small but real subset of these patients [49]. High-dose chemotherapy with stem cell rescue has been used in the setting of progressive or relapsed hepatoblastoma. However, as the available data is based on case reports or small series with potential for selection bias, the role and efficacy of this approach are still unknown [38,50–52]. Hepatic intra-arterial chemoembolization has been shown to be efficacious in shrinking these tumors and allowing complete surgical resection after initial systemic chemotherapy [53,54]. Surgical resection of relapse nodules in the lungs can be curative, but has a high failure rate [55].

Agents like irinotecan and oxaliplatin have been tested in small numbers of patients with relapse [48,56,57]. Whereas irinotecan has shown to have some activity, no objective response was seen for hepatoblastoma in a phase II study of oxaliplatin [57]. Newer targeted agents that 'selectively' interfere with the pathway targets involved in tumor growth, progression, and vascular development, such as insulin-like growth factor (IGF), phosphatidylinositol 3-kinase (PI3K), mammalian target of rapamycin (mTOR), and vascular endothelial growth factor (VEGF), are currently under development. Gene-directed treatment approaches and immunotherapy have high potential as future treatment options. Both therapy options have displayed promising results in preclinical models so far, but are clearly only in the infancy of their scientific evaluation [58–65].

CONCLUSION

Further understanding of the histopathologic subtypes and molecular mechanisms responsible for the development and progression of these tumors is essential to prioritize the most promising agents for clinical evaluation. International cooperation is necessary for the continuous improvement in the outcomes of these patients and the advancement in the knowledge of the genetics, epidemiology, and biology of these tumors. With the foundation provided by the CHIC, work is now well underway in the formation of a new cooperative international hepatoblastoma trial, fostering our ability to compare the historic differences between the chemotherapeutic and surgical approaches of different study groups and define the true state of the art.

Acknowledgements

Funding for the Children's Hepatic tumor International Collaboration (CHIC) has been provided by grants from European Network for Cancer research in Children and Adolescents (ENCCA),FP-7,#261474; Hepatoblastoma Foundation administered through CureSearch; and Japanese Children's Cancer Foundation.

Conflicts of interest

There are no conflicts of interest.

REFERENCES AND RECOMMENDED READING

Papers of particular interest, published within the annual period of review, have been highlighted as:
- ▪ of special interest
- ▪▪ of outstanding interest

1. López-Terrada D, Finegold MJ. Tumors of the liver. In: Suchy FJ, editor. Liver disease in children. New York: Cambridge University Press; 2012.
2. Garber JE, Li FP, Kingson JE, *et al.* Hepatoblastoma and familial adenomatous polyposis. J Natl Cancer Inst 1988; 80:1626–1628.
3. Cohen MM Jr. Beckwith–Wiedemann syndrome: historical, clinicopathological, and etiopathogenetic perspectives. Pediatr Dev Pathol 2005; 8:287–304.